Efficient Infrared Electroluminescent Devices using Solution-Processed Colloidal Quantum Dots**

By *Gerasimos Konstantatos*, *Changjun Huang*, *Larissa Levina*, *Zhenghong Lu*, and *Edward H. Sargent**

We report efficient electroluminescence in the near-infrared from PbS–MEH-PPV (poly(2-methoxy-5-(2′-ethylhexyloxy)-1,4-phenylenevinylene)) large-area, solution-cast nanocomposite devices. We employ multivariate optimization of the structural and materials components that govern the radiative, energy-transfer, and bipolar-injection efficiencies into the devices. As a result, we report an external electroluminescence quantum efficiency of 0.27 %, which corresponds to an internal electroluminescence quantum efficiency of 1.9 %. The very best devices exhibit internal-radiative-efficiency-limited performance and not transport- or capture-limited performance, indicating that further gains in efficiency may be achieved if the internal radiative efficiency of the nanocrystal–polymer composite can be further increased without compromising transfer and device bipolar-injection efficiency.

1. Introduction

Light-emitting diodes based on solution-processed nanocrystals have the potential to offer low manufacturing cost, compatibility with a variety of substrates, quantum-size-effect tunability, and physical flexibility. Solution-processed infrared light emitters that can be integrated on CMOS-processed silicon electronics are of interest in chip-to-chip and board-to-board optical interconnections and in fiber-optic and optical wireless communications. Large-area infrared emitters for biomedical imaging would enable optical diagnosis in the biological transparency windows at 800, 1100, and 1300 nm.

To date, infrared electroluminescence from polymer–nanocrystal devices has been reported with external electroluminescence quantum efficiencies (ELQE) of 0.5 %,[1] but only in materials systems in which core–shell nanocrystal growth is possible. In the PbS and PbSe materials systems, in which only the much simpler homostructure colloidal-quantum-dot synthesis has been demonstrated, external ELQEs have to date been limited to 0.0086 %[2] and 0.001 %.[3] If this limitation could be overcome, then PbS and PbSe colloidal quantum dots, which have now been demonstrated[4] to provide optical gain, photodetection, and photovoltaic effects, all in the infrared, could come to represent a broad platform for solution-processed, integrated infrared optoelectronics.

Here we show for the first time that high external ELQEs can be achieved in an electroluminescent device based on homostructure PbS quantum dots. We increased the external ELQE of homostructure quantum dot infrared electroluminescent devices by more than a factor of thirty relative to previous reports. Rather than work within the single-monolayer-of-dots phase-segregation approach pioneered by Bulovic,[3] which is effective in core–shell nanoparticles but not in the more surface-sensitive and packing-density-dependent homostructure quantum dots system, we instead took the view that electroluminescence efficiency must be maximized systematically as a product of three components:

- The internal radiative efficiency of nanocrystals: photons generated per exciton captured. This arises from the degree of perfection of the semiconductor crystalline material making up the quantum dots and from the completeness of their surface passivation.
- The capture efficiency: excitons captured per exciton generated. This is influenced by the mechanism of excitation: neutral energy transfer, or charge-carrier capture via tunneling through the surface-passivating, insulating ligand barrier. Energy transfer depends on the acceptor–donor distance R as $1/R^6$, with the sole role of the ligand barrier being its additive contribution to the acceptor–donor distance. Tunneling, on the other hand, depends exponentially on the barrier thickness and thus the ligand length. Separate injection of each type of carrier depends on the polymer–nanocrystal heterostructure type (exciton confining vs exciton separating), whereas Förster transfer depends only on overlap of the donor (polymer) emission spectrum with the acceptor (nanocrystal) absorption spectrum.
- The bipolar injection efficiency: excitons generated per carrier injected. Balanced charge-carrier injection and trans-

[*] Prof. E. H. Sargent, G. Konstantatos, L. Levina
The Edward S. Rogers, Sr. Department of Electrical and Computer Engineering
University of Toronto
Toronto, ON M5S 3G4 (Canada)
E-mail: ted.sargent@utoronto.ca
Dr. C. Huang, Prof. Z. Lu
Department of Materials Science and Engineering
University of Toronto
Toronto, ON M5S 3G4 (Canada)

[**] The authors gratefully acknowledge Vlad Sukhovatkin, Ahmed Maria, Fred Chang, and Steve McDonald for providing the equipment for PLQE and photoconductivity measurements. We also thank Prof. Alex Shik for fruitful theoretical discussions. The authors acknowledge Materials and Manufacturing Ontario, a division of the Ontario Centres of Excellence; the Natural Sciences and Engineering Research Council of Canada through its Collaborative Research and Development Program; Nortel Networks; the Canada Foundation for Innovation; the Ontario Innovation Trust; and the Canada Research Chairs Programme.

DOI: 10.1002/adfm.200500379

port are required to ensure efficient bipolar operation with a minimum of overbarrier leakage of one type of carrier.[5] Electron-blocking and hole-blocking layers (heterostructure confinement) keep injected carriers in the active region once injected, and proper anode and cathode design facilitate equal injection in the first instance.

2. Results and Discussion

The devices considered herein are made using PbS nanocrystals capped with the oleate ligands present on the surface of nanocrystals following synthesis; or, in the case of so-called exchanged nanocrystals, a post-synthetic ligand-exchange procedure was followed to replace the oleate with the shorter octylamine ligand. Octylamine has an amine head and an eight-carbon-atom chain, whereas oleic acid is an eighteen-carbon-atom chain molecule with a carboxylic acid group head. Poly(2-methoxy-5-(2′-ethylhexyloxy)-1,4-phenylenevinylene) (MEH-PPV) was used as the polymer matrix. Nanocrystals and the semiconducting polymer were codispersed in toluene for solution processing.

The internal radiative efficiency was investigated through photoluminescence quantum efficiency (PLQE) measurements.[6] A laser at 831 nm excited the nanocrystals exclusively and not the polymer matrix. The PLQE of the octylamine-capped nanocrystals in solution was 7.6 ± 1 %. Films were made using spin-casting and resulted in a PLQE of 0.3 ± 0.1 %. Reasons for the order-of-magnitude decrease include both an increase in the density of unpassivated surface states in the nanocrystals during film formation and also energy transfer from smaller to bigger nanocrystals.[7] Here, we therefore use a host matrix[8] to increase the nanocrystal PLQE. Figure 1A shows the PLQE for different concentrations of polymer matrix (MEH-PPV) to nanocrystals. Figure 1B shows the PL spectra for films of different concentration as well as the PL spectrum of the nanocrystals in solution. In film, there is a significant blue-shift converging towards the solution PL spectrum as the polymer concentration increases. In films made using a low concentration of nanocrystals, PLQE reaches 5 %, an increase of an order of magnitude relative to concentrated nanocrystals. In Figure 1C (1,2) cross-sectional transmission electron microscopy (TEM) images of the polymer–nanocrystal composite films covered with a gold layer are illustrated, confirming close packing at high nanocrystal concentration (Fig. 1C1). As the polymer concentration increases (Fig. 1C2) the nanocrystals disperse more uniformly throughout the film, and they do not form aggregates. The results point to energy-transfer quenching among nanocrystals in the solid state as a contributor to low PLQE in films.

The next component to be optimized is the bipolar carrier-injection efficiency. The parameters varied to this end were the cathode and the thickness of the active layer. The cathode governs both the injection of electrons and confinement of holes, whereas the thickness of the active layer determines the effective capture cross-section.[5] The device structures investigated in this report are shown in Figure 2, and the process is described in detail in the Experimental: one device employed an Mg cathode in direct contact with the active layer, while the other employed an aluminum tris(8-hydroxyquinoline) (Alq_3) electron injection/hole-blocking layer between the Al cathode and the active layer.

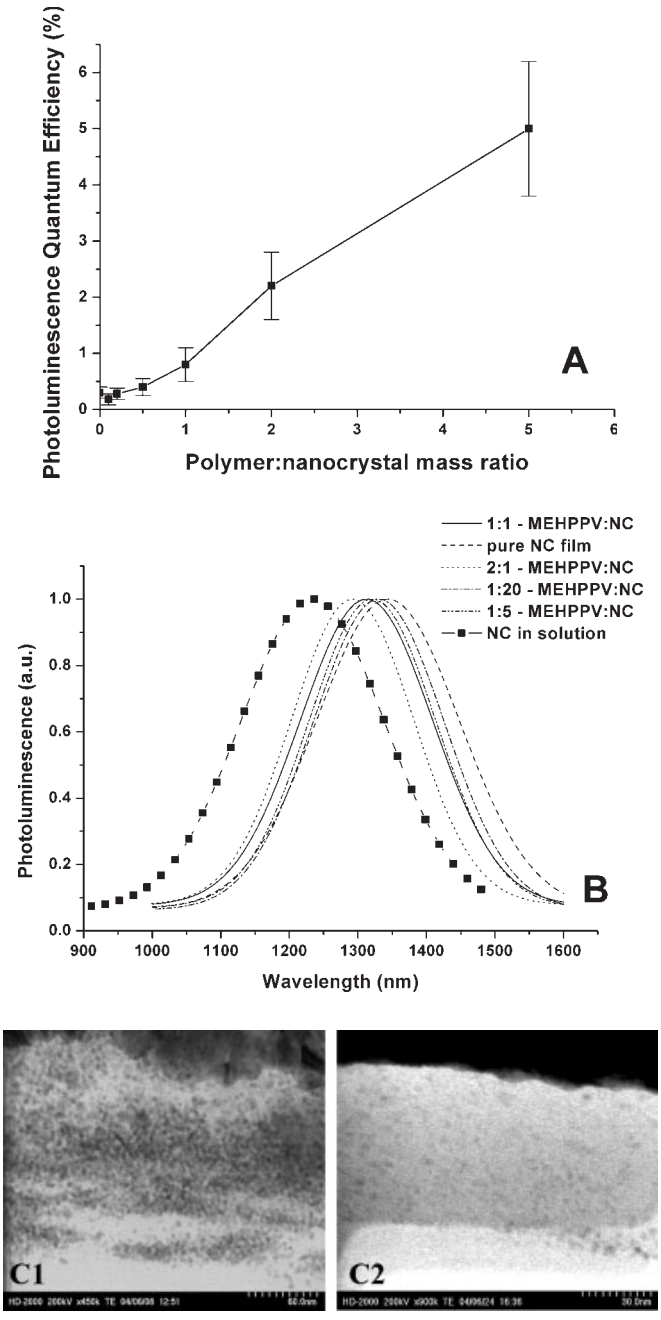

Figure 1. PLQE dependence on polymer/nanocrystal mass ratio. A) The increase in PLQE with increasing polymer concentration. B) The blue-shift in PL spectra towards the solution PL spectrum with increasing polymer concentration. C) Cross-sectional TEM images of two extreme cases of concentration 1) 1:10 and 2) 5:1 polymer/nanocrystal.

Typical electroluminescence (EL) and photoluminescence (PL) spectra of these devices are shown in Figure 3. The EL spectrum from original-nanocrystal devices shows a peak at

ADVANCED FUNCTIONAL MATERIALS

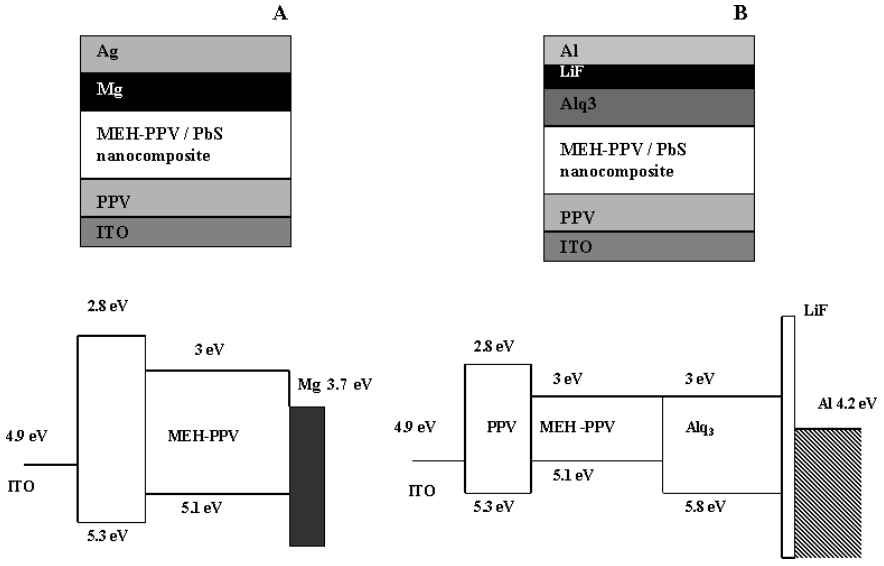

Figure 2. The investigated device structures. A) The Mg-cathode device and the corresponding band diagram in flat-band condition; B) The Alq_3/LiF/Al-cathode device.

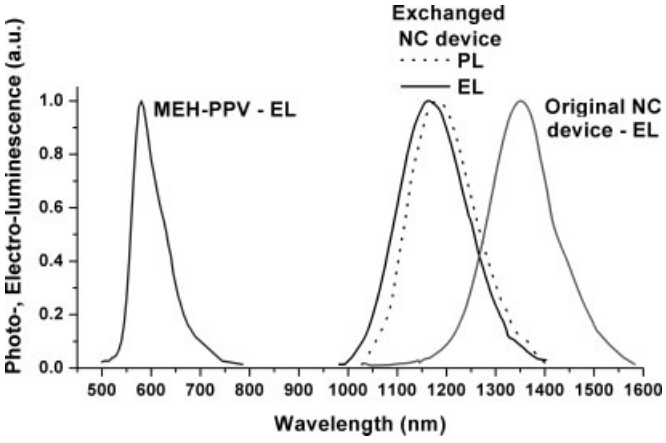

Figure 3. The spectral response of the electroluminescent devices. Infrared and visible emission spectra of the light-emitting diodes are shown. The visible emission at 600 nm stems from MEH-PPV, whereas the infrared emission arises from band-edge emission of the PbS nanocrystals.

1350 nm, whereas the exchanged nanocrystals emit at center wavelength 1160 nm with a full width at half maximum (FWHM) of ~170 nm. The blue-shift in the octylamine-capped nanocrystals arises from the reduction in nanocrystal size accompanying ligand exchange. Orange emission from MEH-PPV at 600 nm is also seen in Figure 3.

Figure 4A shows the light–current–voltage (*L–I–V*) characteristics of a 1:8 (mass ratio) polymer/nanocrystal Mg-cathode device. The reverse bias current consists of holes injected from Mg and moving towards the anode, whereas electrons are not strongly injected from and transported through PPV. The current is thus unipolar, accounting for the lack of observed electroluminescence in spite of a significant reverse current. Figure 4B shows the external ELQE for Mg-based devices of different concentrations and thicknesses. ELQE increases with

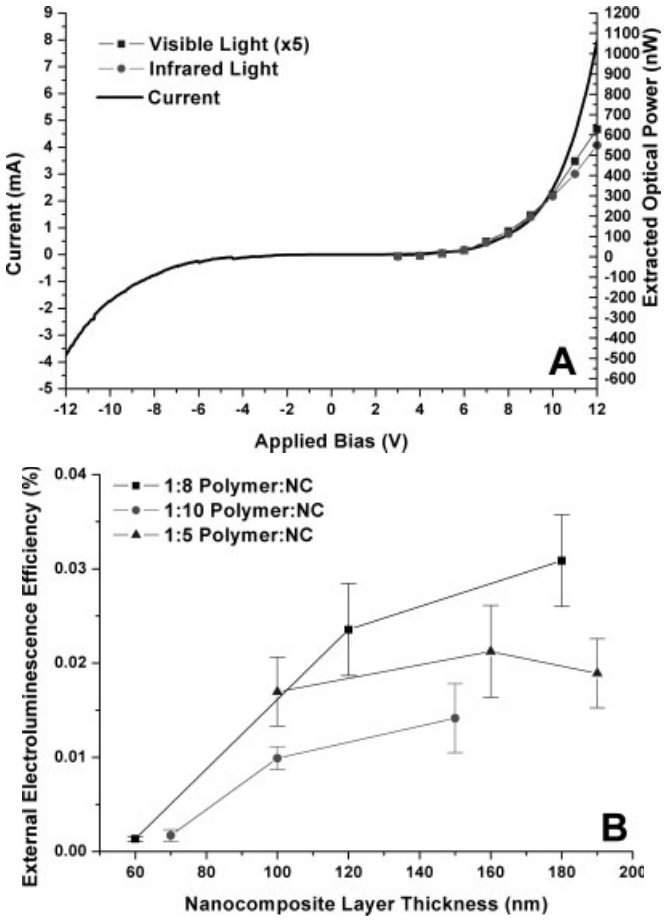

Figure 4. Electro-optical characteristics of the Mg-cathode devices. A) Typical *L–I–V* characteristics of a 1:8 polymer/nanocrystal Mg-cathode device; the visible as well as the infrared extracted optical power are shown. B) External ELQE versus the varied parameters: active layer thickness and polymer/nanocrystal concentration. Mg-devices corresponding to higher PLQE active layer did not emit infrared light.

thickness, up to 180 nm. The thickness of the active layer determines the thickness of the recombination zone, with thicker active layers providing a greater effective capture area for asymmetric structures under strong matrix recombination.[9] Devices with active layer thicknesses greater than 300 nm did not exhibit electroluminescence and required an elevated applied voltage to achieve significant current flow. Figure 4B points to an optimal concentration at a ratio of 1:8 polymer/nanocrystal by mass. Heavily nanocrystal-loaded devices consisted of closely packed, clustered nanocrystals, impeding energy transfer from the polymer to the nanocrystals. As the polymer/nanocrystal mass ratio was increased above 1:8, the efficiency dropped, and no infrared emission was observed for devices with concentrations of 1:2, 1:1, and 2:1 polymer/nanocrystal. These lower-nanocrystal-loading films did, however, exhibit enhanced PLQE, motivating the search for a way to achieve EL emission from such active layers.

We pursued balanced carrier injection to expand the recombination zone throughout the thickness of the device. In Figure 5A, the light–current–voltage characteristics are shown for a 1:1 polymer/nanocrystal device. Alq_3 devices exhibited much stronger rectification than the Mg-contact devices. Under reverse bias, hole injection was suppressed by the LiF barrier and the lack of hole transport through Alq_3. Under forward bias, the extracted optical power was considerably higher than in the Mg-contact case. The infrared emission reached 3.8 μW and the visible emission from MEH-PPV exceeded 8 μW. Figure 5B illustrates the external ELQE versus the active layer thickness and the polymer/nanocrystal concentration. In this case also, the ELQE increases with the thickness and the optimum value appears to lie beyond 200 nm. Beyond 400 nm, optical power output became weak, and the required operating bias exceeded 30 V.

A 2:1 polymer/nanocrystal device exhibited a maximum external infrared ELQE 0.27 % corresponding to an internal infrared ELQE of 1.9 %. The same active material had exhibited PLQE of 2.2 %. The fact that internal ELQE approaches PLQE demonstrates that optimization of transport and capture had been effective, and that the limiting factor in the efficiency of these devices is now internal radiative efficiency of the nanocrystals. In this case, the inter-dot distance is larger than the exciton diffusion length, and excitons formed in the polymer recombined before being captured by the nanocrystals, leading to deterioration in the capture-efficiency component. This effect has been predicted using theoretical modeling.[10]

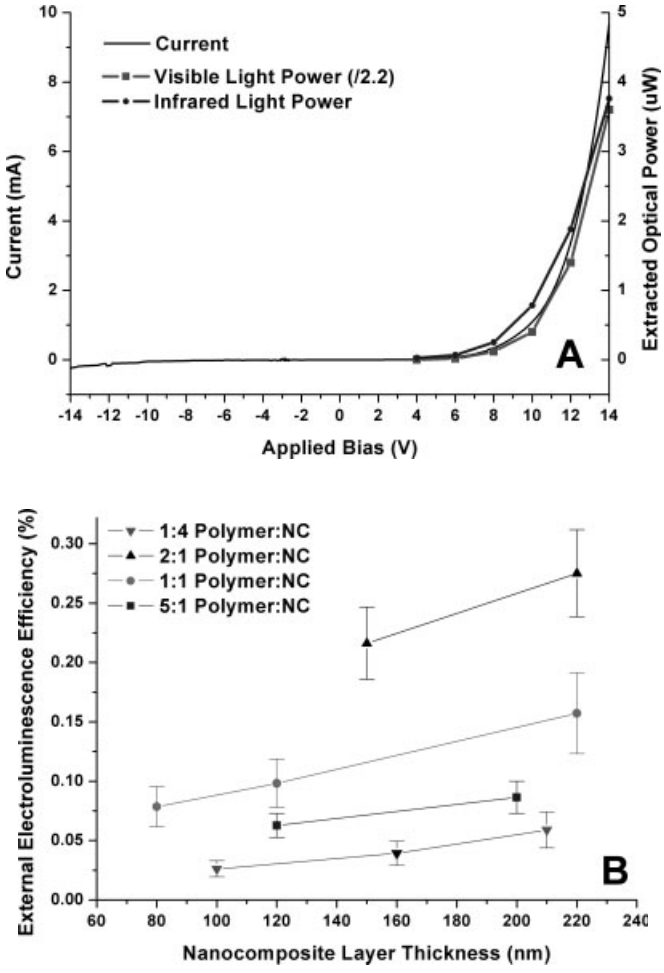

Figure 5. Electro-optical characteristics of the Alq_3/LiF/Al-cathode devices. A) The *L–I–V* characteristics of a 1:1 polymer/nanocrystal Alq_3/LiF/Al device. The rectification is obviously improved compared to the Mg-cathode devices. B) The trends of ELQE dependency on the thickness and the concentration of the active layer. High-PLQE active layers also exhibited high ELQE close to the upper limit of the PLQE.

3. Conclusion

In summary, large-area, solution-processed, infrared light-emitting diodes have been fabricated and investigated, and the efficiency has been analyzed and optimized towards the maximization of overall ELQE. An external ELQE of 0.27 % was achieved, corresponding to an internal ELQE of 1.9 %. The very best devices exhibited internal-radiative-efficiency-limited performance and not transport- or capture-limited performance. This suggests that major further gains are ready to be achieved if PLQE in thin solid nanocrystal–polymer composites can be maximized without compromising transfer and device bipolar-injection efficiency. ELQE, taken together with photoconductivity efficiency measurements,[11] suggested the dominant excitation mechanism to be neutral energy transfer. In this regime, ligand length does not impose a strict limitation on device performance and remains a degree of freedom available for significant further optimization in achieving efficient passivation.

4. Experimental

PbS Nanocrystal Synthesis and Ligand Exchange: PbS nanocrystals were synthesized [12], resulting in nanoparticles capped with oleate ligands. A post-synthetic ligand exchange was employed to replace the oleate ligands with octylamine. The original nanocrystal solution in toluene was precipitated with methanol, dried, and redispersed in an excess of octylamine. The solution was heated at 70 °C for 8 h and then nanocrystals were redispersed in a new portion of octylamine after precipitation with dimethylformamide (DMF) and drying. The solution

ADVANCED FUNCTIONAL MATERIALS

was left at room temperature for 16 h, and the process was repeated. After the second day the solution was precipitated with DMF and dispersed in toluene.

PLQE Measurement: PLQE was taken to be the difference in the photoluminescence-emitted light divided by the difference in the absorbed laser-excitation light between direct and indirect illumination conditions [6]. Special care was taken to ensure that the investigated samples either in solution or film had optical density values smaller than 0.05, corresponding to less than 10 % reabsorption.

Electroluminescent Device Fabrication: Devices were fabricated using a single batch of nanocrystals to facilitate comparison. A 40 nm film of precursor PPV was spin-coated on glass substrates covered by 30 nm of indium tin oxide (ITO). The films were polymerized by annealing for 2 h at 200 °C under vacuum. The PPV layer blocks electrons from overflowing into the ITO and also serves as a hole-transport layer. The use of PPV was also used to eliminate short circuits due to pinholes. MEH-PPV/nanocrystal blends of different concentrations were spin-coated on the PPV to form the active region. The thickness and uniformity of the active layer were determined by the solution viscosity and spin speed. Two types of cathode were fabricated. In one case, 150 nm of Mg was deposited, followed by 100 nm of Ag and 10 nm of Au to protect the Mg. The contacts were circular and of 1 mm radius. The second cathode approach involved evaporation of Alq_3 followed by a 1 nm thin LiF layer and 30 nm of Al. The metallic contact was then protected using 300 nm of Ag. Alq_3 served as an electron-transport and hole-blocking layer. The barrier formed at the highest occupied molecular orbital (HOMO)-level interface of MEH-PPV and Alq_3 prevents hole flow towards the cathode and confines excitons more effectively inside the active region. The LiF/Al contact has been reported to provide efficient electron injection into Alq_3 [13].

Determination of Electroluminescence Quantum Efficiency: The device was placed atop a Newport germanium detector which collected emission through the glass slide. When only infrared integral power was to be acquired, a silicon wafer was placed between device and detector to filter out visible radiation. To account for absorbance and reflectance from silicon, a spectrally resolved transmittance measurement was taken and a correction was applied based on the wafer's absorbance and reflectance spectra. A Lambertian emission pattern was used in accounting for the angular dependence of reflectance.

To estimate the internal ELQE, the ITO, PPV, Alq_3, and active MEH-PPV/nanocrystal layers were assumed to have an effective refractive index of 1.9. Ellipsometry was used to measure the nanocomposite layer, whereas published values were used for MEH-PPV [14], Alq_3 [15], and PPV [16]. The glass substrate was taken to have a refractive index of 1.5 and air refractive index of 1. We assumed a Lambertian emission distribution. The extraction efficiency of light generated within the active layer was calculated by taking into account total internal reflection at the glass/active layer interface.

Optical versus Electrical Pumping in EL Devices: In the devices presented herein, it was necessary to contemplate the possibility that visible emission could excite nanocrystals optically. To investigate this possibility, the device was illuminated with 3.2 mW of 831 nm laser over the device area. The detected PL power, measured using the same setup as the one used to measure ELQE, was less than 15 nW. As a further verification that optical pumping of infrared-emitting nanocrystals inside nanocomposite devices was a negligible factor, we also fabricated devices using only MEH-PPV as the active layer material. The maximum visible EL power was measured to be ~12 μW and the difference between the nanocrystal and non-nanocrystal devices was thus ~5 μW. The exciton generation rate η_{exc} can be estimated as $P_{vis}/h\nu_{vis}$, where P_{vis} is the optical power, ν_{vis} is the light frequency, and h is Planck's constant, and the estimated infrared photoluminescence power calculated ($P_{IR} = \eta_{exc} h \nu_{IR}$ PLQE) equaling ~40 nW. This estimation further confirms that the major part of the generated infrared light stems from transfer excitation rather than radiative excitation.

Received: November 7, 2004
Final version: May 31, 2005

[1] N. Tessler, V. Medvedev, M. Kazes, S. Kan, U. Banin, *Science* **2002**, *295*, 1506.
[2] L. Bakueva, S. Musikhin, M. A. Hines, T.-W. F. Chang, M. Tzolov, G. D. Scholes, E. H. Sargent, *Appl. Phys. Lett.* **2003**, *82*, 2895.
[3] J. S. Steckel, S. Coe-Sullivan, V. Bulovic, M. Bawendi, *Adv. Mater.* **2003**, *15*, 1862.
[4] E. H. Sargent, *Adv. Mater.* **2005**, *17*, 515.
[5] L. Bakueva, S. Musikhin, E. H. Sargent, H. E. Ruda, A. Shik, in *Handbook of Organic–Inorganic Hybrid Materials and Nanocomposites*, Vol. 2 (Ed: H. S. Nalwa), American Scientific Publishers, Stevenson Ranch, CA **2003**.
[6] M. Tzolov, W. Brütting, V. Petrova-Koch, J. Gmeiner, M. Schwoerer, *Synth. Met.* **2001**, *122*, 55.
[7] S. A. Crooker, J. A. Hollingsworth, S. Tretiak, V. I. Klimov, *Phys. Rev. Lett.* **2002**, *89*, 186 802.
[8] T.-W. F. Chang, A. Maria, P. W. Cyr, V. Sukhovatkin, L. Levina, E. H. Sargent, *Synth. Met.* **2005**, *148*, 257.
[9] A. Shik, S. Yu, E. Johnson, H. Ruda, E. H. Sargent, *Solid-State Electron.* **2002**, *46*, 61.
[10] A. Shik, G. Konstantatos, E. H. Sargent, H. E. Ruda, *J. Appl. Phys.* **2003**, *94*, 4066.
[11] S. A. McDonald, G. Konstantatos, S. Zhang, P. W. Cyr, E. J. D. Klem, L. Levina, E. H. Sargent, *Nat. Mater.* **2005**, *4*, 138.
[12] M. A. Hines, G. D. Scholes, *Adv. Mater.* **2003**, *15*, 1844.
[13] J. Yoon, J.-J. Kim, T.-W. Lee, O.-O. Park, *Appl. Phys. Lett.* **2000**, *76*, 2152.
[14] J. A. E. Wasey, A. Safonov, I. D. W. Samuel, W. L. Barnes, *Phys. Rev. B* **2001**, *64*, 205 201.
[15] V. Bulovic, V. B. Khalfin, G. Gu, P. E. Burrows, D. Z. Garbuzov, S. R. Forrest, *Phys. Rev. B* **1998**, *58*, 3730.
[16] R. Burzynski, P. N. Prasad, F. E. Karasz, *Polymer* **1990**, *31*, 1137.

FULL PAPERS

Electroluminescent Devices

G. Konstantatos, C. Huang, L. Levina, Z. Lu, E. H. Sargent* ..... ■ – ■

Efficient Infrared Electroluminescent Devices using Solution-Processed Colloidal Quantum Dots

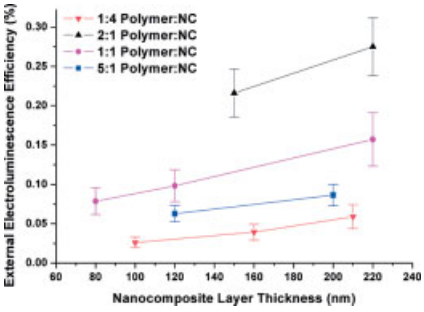

Quantum dot devices: Optimization of the electroluminescence efficiency of near-infrared light-emitting PbS–MEH-PPV large-area, solution-cast nanocomposite devices is reported. External electroluminescence quantum efficiency of 0.27% is obtained (see Figure), corresponding to an internal efficiency of 1.9%. The best devices are limited by the internal radiative efficiency of the nanocrystals (NCs).